RSC Applied Polymers

PAPER

View Article Online
View Journal | View Issue

Cite this: *RSC Appl. Polym.*, 2026, **4**, 839

Impact of π-conjugation and fluorination on the sensing performance of 1,6-pyrene covalent triazine frameworks

M. Carmen Borrallo-Aniceto,[a] Beatriz Fuerte-Díez,[a] Laura González-Aguilera,[a] M. Luisa Ferrer,[a] M. Pilar Lillo,[b] Andreas Mavrandonakis,[a] Urbano Díaz,[c] Eva M. Maya *[a] and Marta Iglesias *[a]

In this work, we describe the synthesis of a series covalent triazine frameworks (CTFs) based on 1,6-substituted-pyrene-derivatives, in which triazine units (electron acceptor groups) are either directly bonded to the pyrene core (1,6-Pyr-CTF) or connected *via* aryl or fluoroaryl-π-linkers (1,6-DPhPyr-CTF and 1,6-2FDPhPyr-CTF). These CTFs were readily synthesized through cyclotrimerization of the corresponding dinitriles, yielding thermally stable products with favorable photophysical properties and fluorescence emission maxima at 401 nm (1,6-Pyr-CTF), 428 nm (1,6-DPhPyr-CTF) and 433 nm (1,6-2FDPhPyr-CTF). These characteristics make them promising candidates for fluorescent sensing of nitroaromatic compounds. Among the synthesized frameworks, the fluorinated diphenylpyrene-triazine (1,6-2FDPhPyr-CTF) exhibits the highest selectivity and sensitivity toward nitro compounds, in EtOH/H_2O dispersions, with K_{SV} = 4.35 × 10^4 M^{-1} (LOD = 0.15 ppm) for picric acid (TNP) or 3.39 × 10^4 M^{-1} (LOD = 0.11 ppm) for (*p*-nitroaniline, 4-NA). These results demonstrate the beneficial effect of extended π-conjugation and fluorine incorporation on the sensing performance of CTFs.

Received 28th November 2025,
Accepted 25th February 2026

DOI: 10.1039/d5lp00381d

rsc.li/rscapplpolym

Introduction

The development of effective methods for the detection of effluents such as nitroaromatic compounds (NACs), which are commonly used in explosives,[1,2] is of great importance in both environmental and biological fields.[3,4] There are several methods for detecting explosives and/or ions, including ion mobility,[5] mass spectrometry,[6] chromatography,[7] Raman spectroscopy[8] and electrochemical sensing.[9] In recent years, fluorescence detection methods have become very attractive because they are easy to use, inexpensive and have excellent sensitivity and selectivity for the detection of different compounds.[10–15]

Covalent triazine frameworks (CTFs) are a well-known type of organic frameworks consisting of triazine units covalently bonded to different aromatic nodes, which have become increasingly attractive since they were first reported[16–20] CTFs have highly robust structures with attractive properties such as high thermal and chemical stability, high nitrogen content and porosity. These properties make CTFs attractive for promising applications including molecular recognition,[21] catalysis,[22–26] energy storage,[27,28] environmental remediation,[29–31] gas separation and storage,[32,33] and have provided a suitable platform for the chemical detection of hazardous compounds and ions.[13,15,34–36] Pyrene molecule is a polycyclic aromatic hydrocarbon (PAH) characterized by a long excited-state lifetime, and excellent emission properties, high photochemical and thermal stability.[37–40] Due to its special properties, it has been used as structural building block for the synthesis of pyrene-based derivatives for applications in optoelectronics (organic photovoltaic cells (OPV), dye-sensitized solar cells (DSSCs), organic light-emitting diodes (OLEDs), nonlinear optical (NLO)).[41–44] Pyrene compounds have also applied as sensors for temperature,[45] pH,[46,47] or metal ions[48,49] The functionalization of the pyrene nucleus with electron donor or acceptor groups combined with the extension of π-conjugation allows the control of the electronic properties of pyrene-based compounds, resulting in their wide range of applications.[50–52] The most reactive positions for functionalizing the pyrene core are 1, 3, 6, and 8. Different acceptor groups such as nitro, cyano, cyanoacrylonitrile, and cyanoacrylic acid have been attached to the pyrene moiety at these positions through different π-conjugated linkers, and their resulting properties and applications have been reported.[42,53] It has also been

[a]*Instituto de Ciencia de Materiales de Madrid. CSIC, C/Sor Juana Inés de la Cruz, 3, 28049 Madrid, Spain. E-mail: eva.maya@csic.es, marta.iglesias@icmm.csic.es*
[b]*Instituto de Química Física Blas Cabrera. CSIC, C/Serrano, 119, 28006 Madrid, Spain*
[c]*Instituto de Tecnología Química, Universitat Politècnica de València, Consejo Superior de Investigaciones Científicas, Avenida de los Naranjos s/n, E-46022 Valencia, Spain*

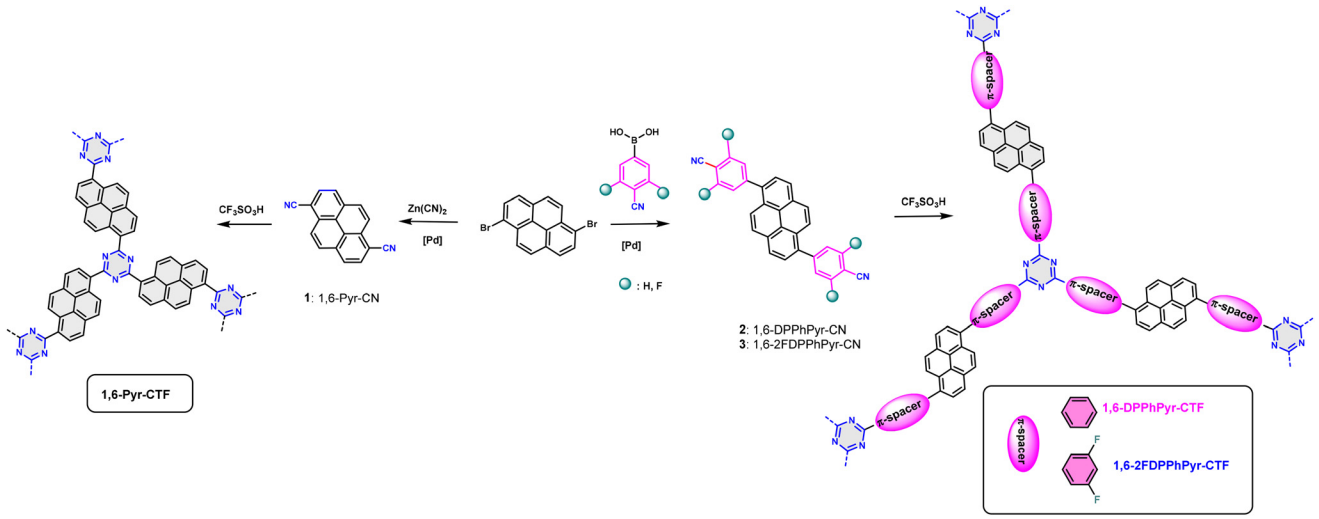

Scheme 1 Synthesis of 1-6-pyrene-based triazines (1,6-Pyr-CTF, 1,6-DPPhPyr-CFT and 1,6-2FDPPhPyr-CTF).

reported that the incorporation of fluorine atoms on the acceptor group can modulate the energy levels of organic dyes,[54] and this effect has been demonstrated by Gao *et al.*, who reported that perfluorobenzonitrile-substituted pyrenes exhibited enhanced properties such as stronger electron-withdrawing ability, greater thermal stability and improved fluorescence compared to perfluorotoluyl-pyrene derivatives.[55]

Recently, we reported the synthesis of a family of 2,7-substituted pyrene-based covalent triazine frameworks (CTFs) and demonstrated their dual detection capabilities. By extending conjugation through the 2,7-positions of the pyrene ring, these materials exhibited excellent fluorescence responses toward dichloran (DCNA), picric acid (PA), and metal ions such as Au^{3+} and Fe^{3+}.[56] In the present work, we focus on a new design strategy by synthetizing 1,6 pyrene-substituted-CTFs, in which the electron-acceptor triazine units are either directly attached to the pyrene core (1,6-Pyr-CTF) or connected *via* π-conjugated phenyl or fluoroaryl groups (1,6-DPhPyr-CTF, 1,6-2FDPhPyr-CTF) (Scheme 1). In the latter, two fluorine atoms are positioned *ortho* to the phenyl ring, acting as additional electron-withdrawing groups. This modification enhances the electron-acceptor character of the framework, promotes charge transfer, and reduces the HOMO–LUMO energy gap.

By shifting the substitution pattern from 2,7- to 1,6-positions and incorporating tunable electron-withdrawing groups, the current design explores a distinct electronic configuration and charge-transfer pathway, highlighting a new structure–property relationship that is different from our previous 2,7-pyrene CTFs.

Results and discussion

Synthesis and characterization of pyrene-based covalent triazine frameworks

1,6-Pyrene-based triazines were easily obtained by trifluoromethanesulfonic acid-catalyzed cyclotrimerization of the corresponding 1,6-pyrenedinitriles (1,6-Pyr-CN, 1,6-DPPhPy-CN and 1,6-2DPPhPy-CN) as shown in Scheme 1.[56] Dinitriles **1** and **2** were synthesized following previously reported methods with some modifications whose details can be found in the SI (Scheme S1).[55,57–60] In contrast, dinitrile **3** is described here for the first time. Pyrene-1,6-dicarbonitrile (1) was synthesized *via* nucleophilic substitution of bromine atoms in 1,6-dibromopyrene with cyano groups using $Zn(CN)_2$ as the cyanine source and [1,1′-bis(diphenylphosphino)ferrocene]dichloropalladium(II) as the catalyst. 4,4′-(pyrene-1,6-diyl)dibenzonitrile (2) and 4,4′-(pyrene-1,6-diyl)bis(2,6-difluorobenzonitrile) (3) were obtained *via* Suzuki–Miyaura cross-coupling of 1,6-dibromopyrene with the corresponding arylboronic acid, (4-cyanophenyl)boronic acid, and (2,6-difluoro-4-cyanophenyl)boronic acid, respectively. FT-IR spectra (Fig. S1–S3) show the characteristic ν (C≡N) stretching vibrations bands at 2223 cm^{-1} for dinitriles **1** and **2**, and 2237 cm^{-1} for compound **3**. In addition, the spectrum of compound **3** shows a distinct C–F stretching band at 1030 cm^{-1}, confirming the presence of fluorine substituents. The ^{1}H-NMR spectra (Fig. S1–S3) exhibit the characteristic chemical shifts of the pyrene rings protons at 8.68 and 8.41 ppm for dinitrile **1**, 8.27 and 8.11 ppm for **2**, and 8.48 and 8.34 ppm for **3**. ^{13}C NMR spectra (Fig. S1–S3) show the nitrile carbon signals (CN) at 116.8, 110.4 and 112 ppm for monomers **1–3** respectively. Compound **3** exhibits a signal at 162.2 ppm corresponding to the C–F bond along with the corresponding signal at −105.57 ppm in its ^{19}F-NMR spectrum (Fig. S3), confirming the presence of fluorinated aryl groups. Thermogravimetric analyses (TGA) indicate that 1,6-pyrene-dinitriles possess good thermal stability with the decomposition temperatures of 300 °C, 380 °C, and 375 °C for compounds **1** to **3**, respectively.

Dinitriles were successfully used to obtain the corresponding 1,6-pyrene-based triazines in high yields. The elemental analysis is in close agreement with the theoretical values (Table S1).

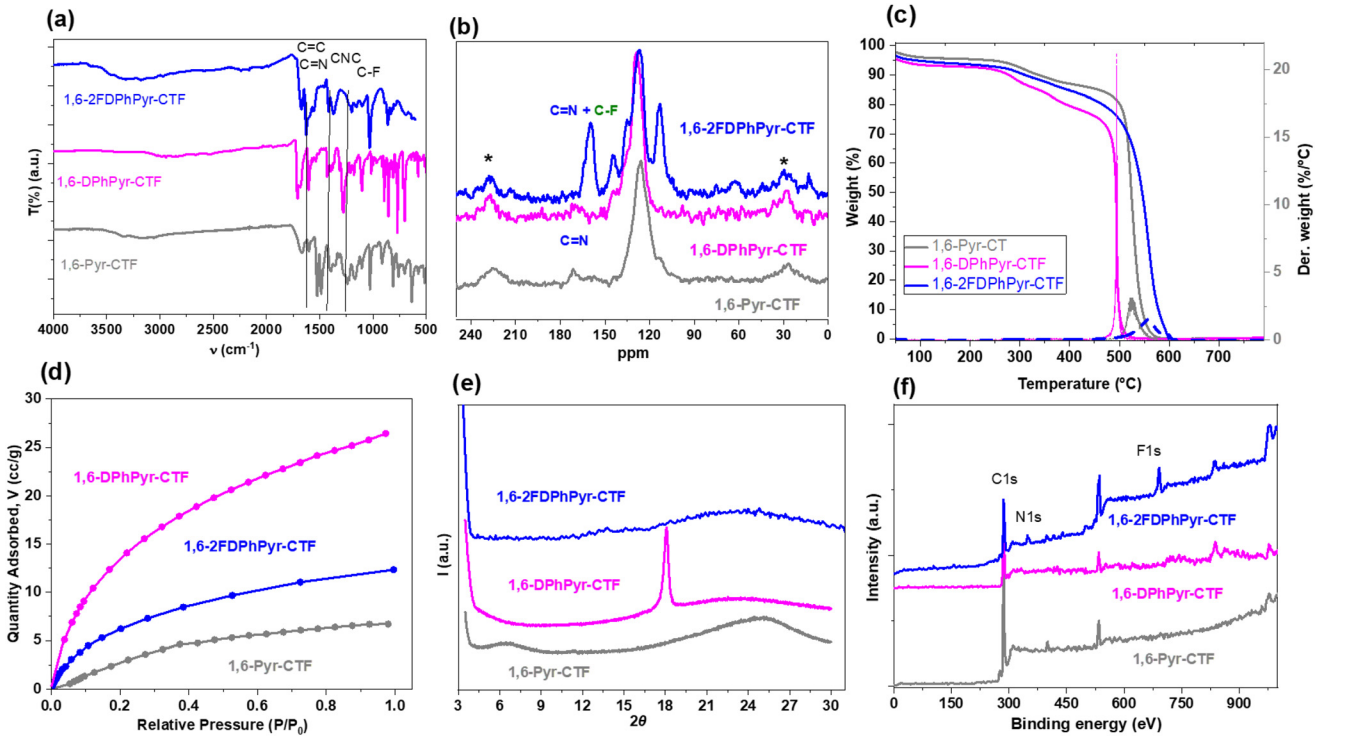

Fig. 1 Characterization data of 1,6-pyrene-based CTFs. (a) FT-IR spectra; (b) ^{13}C-NMR spectra; (c) TGA; (d) CO_2 sorption; (e) PXRD and (f) XPS survey.

The FT-IR spectra (Fig. 1a) show the characteristic bands corresponding to the pyrene core, the aromatic rings, and the triazine units. Fluorinated-CTF exhibits the C–F band at 1022 cm^{-1}. In addition, the disappearance of the CN stretching band at 2220 cm^{-1} confirms the formation of the covalent triazine framework (Fig. S4). The fluorinated-1,6-2FDPhPyr-CTF exhibits two Raman bands at ~1590 cm^{-1} (G-band of sp^2-hybridized carbon) and D-band at ~1350 cm^{-1} assigned to sp^2-hybridized carbon atoms containing structural defects (Fig. S5). The solid-state ^{13}C-NMR (CP-MAS) spectra showed the characteristic resonance of the triazine carbon at approximately 170 ppm. In the fluorinated CTF spectrum, an additional signal is observed at around 165 ppm.

The signals corresponding to aromatic carbons from the pyrene and aryl groups are observed in the region between 100 ppm and 140 ppm (Fig. 1b). Importantly, the absence of the CN signal confirms complete conversion of the dinitrile precursors into the framework. TGA performed under an air atmosphere also indicates that 1,6-pyrene-based CTFs exhibit excellent thermal stability with a major decomposition step occurring around 500 °C (Fig. 1c).

All materials show a Lorentzian signal in their EPR spectra, indicative of the presence of unpaired electrons (Fig. S6). The most intense signal is observed for 1,6-2FDPhPyr-CTF, suggesting a higher concentration of centers with unpaired spins (radicals/defects) in this material.

The porosity of the materials was studied using nitrogen adsorption/desorption isotherms at 77K. Brunauer–Emmett–Teller (BET) surface area analysis revealed values below 20 m^2 g^{-1} for all materials, except for 1,6-DPhPyr-CTF, which exhibited a higher surface area of 75 m^2 g^{-1} (Fig. S7). Additionally, CO_2 adsorption capability was evaluated from the sorption isotherms measured at 273 K and pressures up to 1 atm. The surface areas calculated from the CO_2 adsorption isotherms using the Dubinin–Astakhov (DA) method were 192.5, 81.4, and 121.8 m^2 g^{-1} for 1,6-Pyr-CTF, 1,6-DPhPyr-CTF and 1,6-2FDPhPyr-CTF, respectively. The CO_2 uptake ranged from 0.276 mmol g^{-1} for 1,6-Pyr-CTF to 1.149 mmol g^{-1} for 1,6-2FDPhPyr-CTF (Table 1, Fig. 1d). These results indicate the good affinity of acidic CO_2 molecules for the basic triazine units present in the framework. The polymer 1,6-2FDPhPyr-CTF has a water contact angle of 65.4° (Fig. S8), indicating a moderately hydrophilic surface.

The XPS survey spectra of 1,6 pyrene-based CTFs are shown in Fig. 1f and the corresponding high-resolution C 1s, N 1s, O

Table 1 CO_2 uptake parameters

CTFs	$S_{Langmuir}$ [a] [m^2 g^{-1}]	V_o [cm^3 g^{-1} STP]	CO_2 [mmol g^{-1}]
1,6-Pyr-CTF	192.50	6.69	0.276
1,6-DPhPyr-CTF	81.40	26.43	1.149
1,6-2FDPhPyr-CTF	121.18	24.118	0.551

[a] At 273 K, Dubinin–Astakhov (DA) method; STP: standard temperature and pressure.

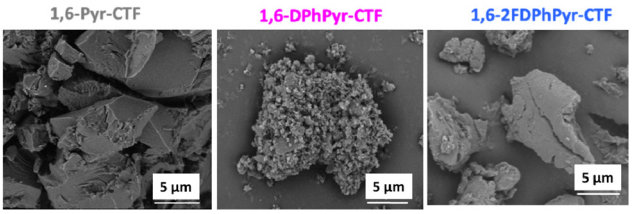

Fig. 2 SEM images of 1,6-pyrene-based CTFs.

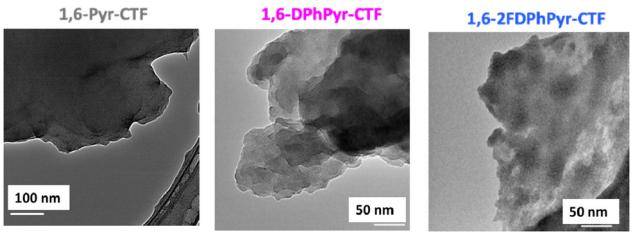

Fig. 3 TEM images of 1,6-pyrene-based CTFs.

1s, and F 1s traces are shown in Fig. S9. In the C 1s spectrum, two main components at binding energies (BE) of ~285–286 eV and ~289–290 eV corresponding to C=C and C=N bonds, respectively, can be observed. The N 1s spectrum showed one type of nitrogen with BE ranging from 399.3 eV to 399.7 eV Additionally, 1,6-2FDPhPyr-CTF shows a peak at 691.4 eV in the F 1s spectrum, confirming the presence of fluorinated groups.

SEM and TEM analyses (Fig. 2 and 3) reveal irregular agglomerates composed of dense, nanosized particles, consistent with the low N_2-BET surface areas measured. The TEM images reveal predominantly amorphous domains with locally ordered lamellar regions, indicating partial π–π stacking between aromatic layers.

This short-range order correlates with the broad diffraction band observed by PXRD (Fig. 1e) and, for 1,6-DPhPyr-CTF, with a reflection centred at $2\theta \approx 18°$, probably corresponding to an interlayer spacing of ~4.9 Å. Such spacing suggests loose aromatic stacking modulated by the phenyl connectors. In contrast, 1,6-Pyr-CTF and 1,6-2FDPhPyr-CTF exhibit fully amorphous patterns, in agreement with their more disordered morphology seen by TEM. Overall, the combined microscopy and XRD data indicate poorly crystalline networks with limited local stacking, which could still promote efficient charge-transfer pathways relevant to their sensing performance.

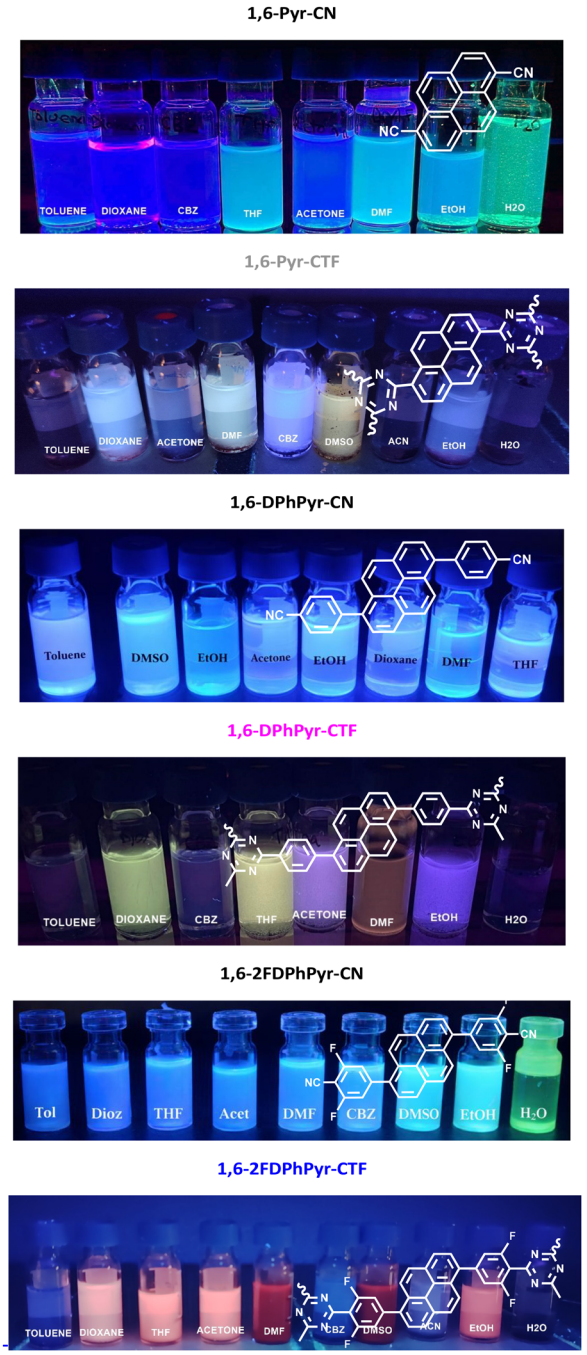

Fig. 4 Fluorescence colour changes of dinitriles and their corresponding 1,6-Pyrene-based CTFs dispersed in different solvents (0.1 mg mL^{-1}), under UV light (λ = 365 nm).

Optical properties

The 1,6-pyrene-based CTFs and their parent dinitriles were dispersed in solvents of varying polarity to investigate their photoluminescent behaviour. Upon excitation with UV light (365 nm), the 1,6-pyrene-based CTFs emitted fluorescence in different colors, whereas the parent dinitriles emitted blue fluorescence (Fig. 4).

The solid-state UV/visible spectra of the 1,6-pyrene-based CTFs showed strong and broad absorption bands extending across the visible region (Fig. 5a), with a pronounced red shift in the absorption maxima compared to the parent dinitriles. This shift is attributed to the formation of extended π-conjugated network within the CTFs (Fig. S10).

The emission spectrum of 1,6-pyrene-based CTFs in different solvents (Fig. 5b) showed the highest fluorescence intensity in ethanol (EtOH) and the lowest in water. To identify a solvent compatible with real sample applications, various

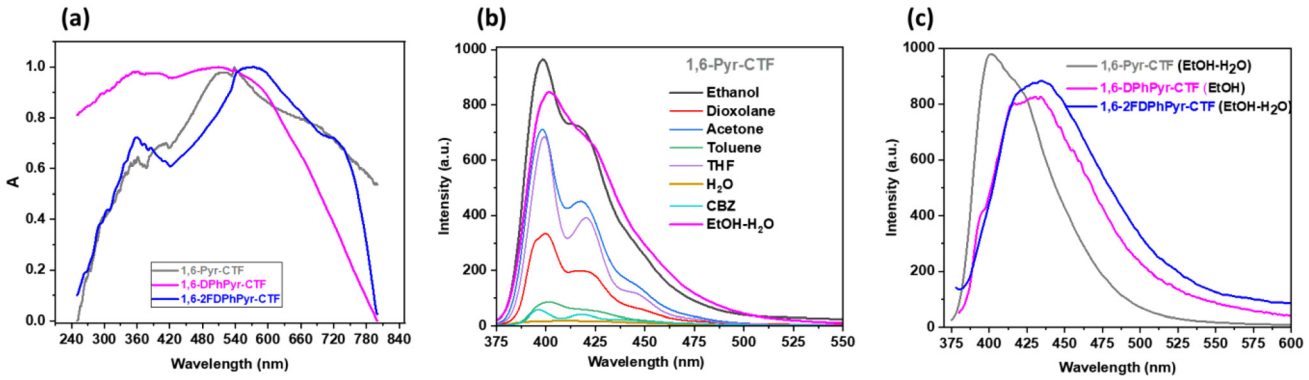

Fig. 5 (a) Normalized solid-state UV-visible absorption spectra; (b) variation in emission spectra in different solvents (0.3 mg/3 mL, λ_{exc} = 352 nm); (c) fluorescence emission spectra (in EtOH–H_2O mixtures) of 1,6-pyrene-based CTFs (λ_{exc} = 352 nm).

EtOH–H_2O mixtures were evaluated. A 1 : 1 EtOH–H_2O mixture was found to provide an optimal balance between fluorescence intensity and dispersion stability (Fig. S11). Fig. 5c shows the fluorescence emission spectra recorded in EtOH–H_2O (1 : 1) mixture with maxima at 401 nm for 1,6-Pyr-CTF, and 433 nm for 1,6-2FDPhPyr-CTF. For 1,6-DPhPyr-CTF, which showed no measurable signal in EtOH–H_2O mixture, the emission spectrum was recorded in pure EtOH, displaying a maximum at 428 nm.

Sensing performance toward nitroaromatic compounds (NACs)

Given the intrinsic properties of covalent triazine frameworks (CTFs) and the electron-deficient nature of nitroaromatic compounds (NACs), which can interact with CTFs and thereby quench their fluorescence,[61] we investigated the potential of pyrene-substituted CTFs as fluorescent chemosensors for a series of NACs with different functional groups (OH, NH_2, halogen, *etc.*).

To assess the influence of pyrene substitution at positions 1,6 *versus* 2,7 on the sensing behavior of the resulting materials, it is important to consider the dispersibility of the materials in solvents of different polarities and the intensity of their corresponding emission spectra.

The emission spectra of the 2,7-series indicated that the highest intensity is observed in solvents such as toluene, dioxolane, and a 1 : 1 dioxolane–water mixture.[56] However, as mentioned above, the emission spectra of 1,6-Pyr-CTF in solvents of varying polarity revealed that the highest intensity corresponds to ethanol or an ethanol–water mixture (1 : 1), while the intensity in dioxolane is only half as strong (Fig. 5b). Therefore, a comparative study between the two series cannot be directly conducted, as each exhibits optimal behavior in solvents with different characteristics, with polar solvents being more favorable in the case of the 1,6-series.

Fluorescence quenching experiments were carried out by adding solutions of the analyte (NAC) to dispersions of the corresponding sensor (0.3 mg/3 mL) in the appropriate solvent (HPLC grade). The quenching behavior was analyzed using the Stern–Volmer (SV) equation ($I_0/I = 1 + K_{SV}[C]$), where I_0 and I are the fluorescence intensities of sensor before and after analyte addition, respectively, and [C] is the analyte molar concentration. From the linear fitting of SV plot at low analyte concentrations, the quenching constant (K_{SV}, M^{-1}) was determined. The detection capability of the 1,6-Pyr-CTF series was studied in the ethanol–water mixture, a solvent with greater potential for detecting contaminants in real-world samples. We first evaluated the sensing performance of 1,6-Pyr-CTF toward a range of NACs (Fig. 6a and Table S2). The highest K_{SV} values were observed for NACs containing amine groups in the *para* position relative to the nitro group specifically 4-nitroaniline (4-NA), dicyanoaniline (DCNA), and 2-amino-5-nitrophenol (2A-5NP), with values of 3.08 × 10^4 M^{-1}, 2.29 × 10^4 M^{-1}, and 1.84 × 10^4 M^{-1}, respectively. The particularly strong response

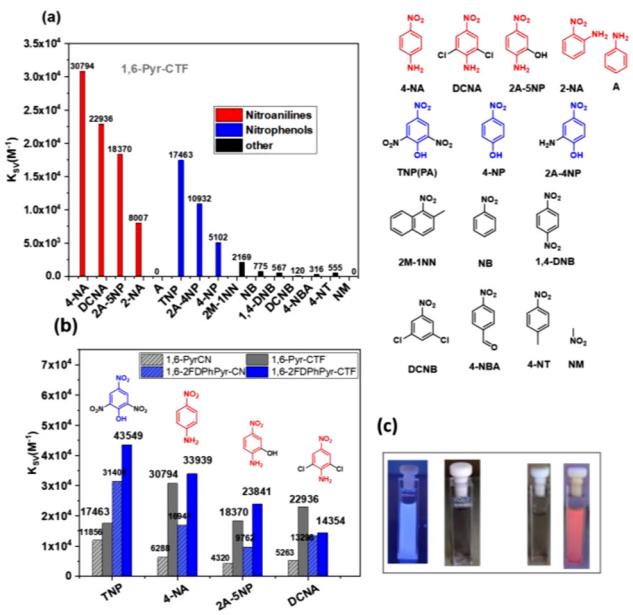

Fig. 6 (a) 1,6-Pyr-CTF response toward NACs; (b) comparison of quenching performance between parent dinitriles and CTFs. (c) Visual response of 1,6-Pyr-CTF and 1,6-2FDPhPyr-CTF in the presence of TNP under UV illumination (365 nm).

toward 4-NA is attributed to its high dipole moment and hyperpolarizability, which facilitate strong interactions with the CTF framework, including N–H and hydrogen bonding interactions. Furthermore, the distinct quenching behaviour of 4-NA compared with other nitroaniline isomers, such as 2-NA, highlights the potential of the CTFs for selective discrimination among structurally similar NACs.

A second group of NACs includes those bearing hydroxyl groups in the *para* position relative to the nitro group—namely TNP, 2A-4NP, and 4-NP—with K_{SV} values of 1.75×10^4 M^{-1}, 1.09×10^4 M^{-1}, and 0.50×10^4 M^{-1}, respectively. In contrast, 1,6-Pyr-CTF exhibited negligible fluorescence quenching in the presence of nitro derivatives such as nitrobenzene (NB) and 1,4-dinitrobenzene (1,4-DNB), as well as other aromatic compounds like toluene, indicating high selectivity. As shown in Fig. 6a, the presence of an amine group has a more pronounced effect on quenching than nitro or hydroxyl groups alone. Furthermore, 1,6-Pyr-CTF demonstrated the highest quenching efficiency when the NAC contained both nitro and amine groups, highlighting its sensitivity to strong electron-donating/electron-withdrawing combinations. Based on these findings, we further examined the sensing behavior of the D-π-A type CTF, 1,6-2FDPhPyr-CTF, toward selected NACs, including TNP, 4-NA, DCNA, and 2A-5NP. Reproducible data could not be obtained with 1,6-DPhPyr-CTF because it does not disperse well in an ethanol-water mixture. For this reason, we only studied the sensing performance of 1,6-2FDPhPyr-CTF. In this case, significantly higher K_{SV} values were obtained compared to 1,6-Pyr-CTF (Fig. 6b), with the best response observed for TNP ($K_{SV} = 4.35 \times 10^4$ M^{-1}). For comparison, the sensing performance of corresponding parent dinitriles was also evaluated, revealing substantially lower quenching responses than those observed for the CTFs. This highlights the enhanced sensing capability provided by the framework structure.

The quenching efficiency (QE) for TNP was found to be 82.8% with 1,6-Pyr-CTF and 86.5% with 1,6-2FDPhPyr-CTF. For DCNA, the QE values were 84.2% and 68.0%, respectively, while for 4-NA the QE reached 82.8% and 91.4% (Fig. S12). To further investigate the sensing behaviour, fluorescence intensity was measured as a function of analyte concentration (Fig. S13). Upon the addition of 149 μmol L^{-1} or 165 μmol L^{-1} of TNP or 165 μmol L^{-1} of 4-NA, the fluorescence of both 1,6-Pyr-CTF and 1,6-2FDPhPyr-CTF was almost completely quenched (QE > 93%), indicating highly efficient detection. Fig. 6c visually confirms that under UV illumination (365 nm), the fluorescence of both materials is fully suppressed upon exposure to TNP, demonstrating their practical potential applicability for NAC detection. Selectivity studies (Fig. S14) further show that in the presence of 4-NA or TNP, the quenching response toward other anilines or phenols is significantly lower, underscoring the high selectivity of both CTFs for target NACs.

The limit of detection (LOD) was calculated using the equation LOD = $3\sigma/\rho$. where σ is the standard deviation of the fluorescence intensity of blank samples (based on 10 replicates) and ρ is slope of the calibration curve (relative fluorescent intensity *vs.* analyte concentration).[62] The LOD values for 1,6-Pyr-CTF and 1,6-2FDPhPyr-CTF were 0.25 and 0.15 ppm for TNP and 0.31 and 0.11 ppm for 4-NA (Table S2). These results confirm the potential of these CTFs for the sensitive detection of 4-NA or TNP in environmental samples. A comparative summary of reported data for triazine-based small molecules and various polymeric organic frameworks is provided in Table S4. The detection capabilities of 1,6-pyrene-based CTFs are comparable to those of other reported materials, with K_{SV} values on the order of 10^4 M^{-1} and limits of detection at the ppm level. Particularly, this work demonstrates how the combination of donor and acceptor units, along with the introduction of functional groups such as fluorine (F), can effectively modulate the properties of a material, in this case, a sensor, to achieve optimal performance.

Finally, the recyclability of both CTFs was studied. As it can be observed in Fig. S15a and S15b, the recovered CTF retained nearly their original fluorescence intensity and maintained consistent sensing performance over at least five cycles for 1,6-Pyr-CTF and three cycles for 1,6-2FDPhPyr-CTF, which indicates the good stability and reusability of both CTFs for the detection of 4-NA or TNP. Additionally, Fig. S15c displays the IR spectra of the recovered samples after the sensing experiments, confirming the preservation of the framework structure.

Mechanisms for nitroaromatic compounds NAC detection

NAC compounds contain electron-withdrawing groups ($-NO_2$), which confer high electronic affinity, strong electronegativity, and notable reduction potential. Among the proposed mechanisms for fluorescence quenching, the photoinduced electron transfer (PET) process, involves quenching *via* electron transfer from the lowest unoccupied molecular orbital (LUMO) level of the donor triazine framework to the LUMO of the NAC acceptor upon photoexcitation.[35] To evaluate the feasibility of this mechanism, the energy levels of the 1,6-Pyr-CTFs derivatives were calculated. First, the optical band gaps were determined using the Kubelka–Munk function derived from the Tauc plot based on diffuse reflectance spectra (Fig. S16 and S17).

The band-gap values obtained were 1.68 eV, 1.75 eV, and 1.72 eV for 1,6-Pyr-CTF, 1,6-DPhPyr-CTF and 1,6-2FDPhPyr-CTF, respectively. Fig. 7a, shows the HOMO–LUMO energy levels estimated from cyclic voltammetry (CV) measurements (Fig. S18 and Table S3). As shown, the LUMO energy levels of all Pyr-CTFs are higher than those of TNP (−3.89 eV) and 4-NA (−3.71 eV), enabling efficient electron transfer from the photoexcited CTF to these analytes. In contrast, the LUMO level of DCNA (−3.01 eV) lies above those of the CTFs, making PET less favourable in this case.

To gain deeper insight into the fluorescence quenching mechanism, Fig. S19 shows the spectral overlap between the emission spectra of 1,6-Pyr-based CTFs and the absorption spectra of various nitro compounds. A significant overlap is observed for TNP, 4-NA, 2A-5NP, and DCNA, while negligible overlap is found for the other analytes tested. This suggests that resonance energy transfer (RET)[63] may also contribute to the quenching process.

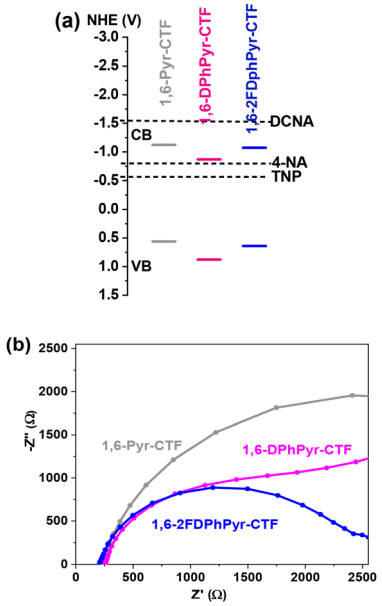

Fig. 7 (a) Energy level diagrams (LUMO from onset reduction potentials $E_{redonset}$) and (b) Nyquist plot from electrochemical impedance spectroscopy (EIS measurements) of 1,6-Pyr-based CTFs.

To further investigate charge separation and transfer properties, electrochemical impedance spectroscopy (EIS) was performed (Fig. 7b). The Nyquist plots reveal that 1,6-2FDPhPyr-CTF exhibits a smaller semi-circular radius compared to its non-fluorinated counterpart, indicating lower charge transfer resistance. Taken together, these data suggest a discrepancy between the LUMO energy levels of 1,6-pyrene-based CTFs and certain NACs during the quenching process, particularly in their limited response toward DCNA. This implies that fluorescence quenching is not governed exclusively by PET.

Additional mechanisms may contribute to the observed quenching behaviour, including ground-electrostatic interaction between the triazines and analytes,[64] resonance energy transfer processes (RET),[65] or inner filter effect (IFE)[66] due to spectral overlap. These findings underscore the complex interplay of structural, electronic, and intermolecular factors that influence the sensing performance of 1,6-pyrene-based CTFs.

To explain the mechanism more, time-resolved fluorescence experiments were conducted (Fig. 8a). The average fluorescence lifetimes obtained were 4.0 ns, 2.5 ns and 1.4 ns for 1,6-Pyr-CTF, 1,6-DPhPyr-CTF and 1,6-2FDPhPyr-CTF respectively. Upon addition of TNP, the lifetimes remained nearly unchanged ($\langle\tau\rangle$ = 2.3 ± 0.3 ns and $\langle\tau\rangle$ = 1.4 ± 0.3 ns) before and after analyte addition (Fig. 8b and c) confirming a static quenching mechanism. Considering these data and previous findings,[67] these results suggest that the selectivity and sensitivity of 1,6-pyrene-based CTFs toward TNP likely arise from the combined contribution of multiple mechanisms[64] including PET, RET and IFE.[66] This highlights the complex interplay of structural, electronic, and intermolecular factors governing the sensing performance of these materials.

Density Functional Theory (DFT) calculations. Considering the experimental results and the preceding, we gained further insights through Density Functional Theory (DFT) calculations.

These calculations offer theoretical explanations for the interfacial interactions involved in the adsorption of nitroaromatic compounds in 1,6-Pyr-based CTFs. For this study, we selected 1,6-Pyr-CTF and 1,6-2FDPhPyr-CTF as sensors and 4-NA and 4-NP as representative analytes due to their structural similarity and the presence of distinct functional groups, an amino group in 4-NA and a hydroxyl group in 4-NP, which allowed us to investigate the influence of different substituents on the sensing behavior. As a 1,6-Pyr-CTF model, we chose a molecular model that consists of a triazine core, which is further extended by three (dimethyl-triazinyl)-pyrene groups, as shown in the top part of Fig. 9. The molecular model for the 1,6-2FDPhPyr-CTF has been constructed in a similar manner.

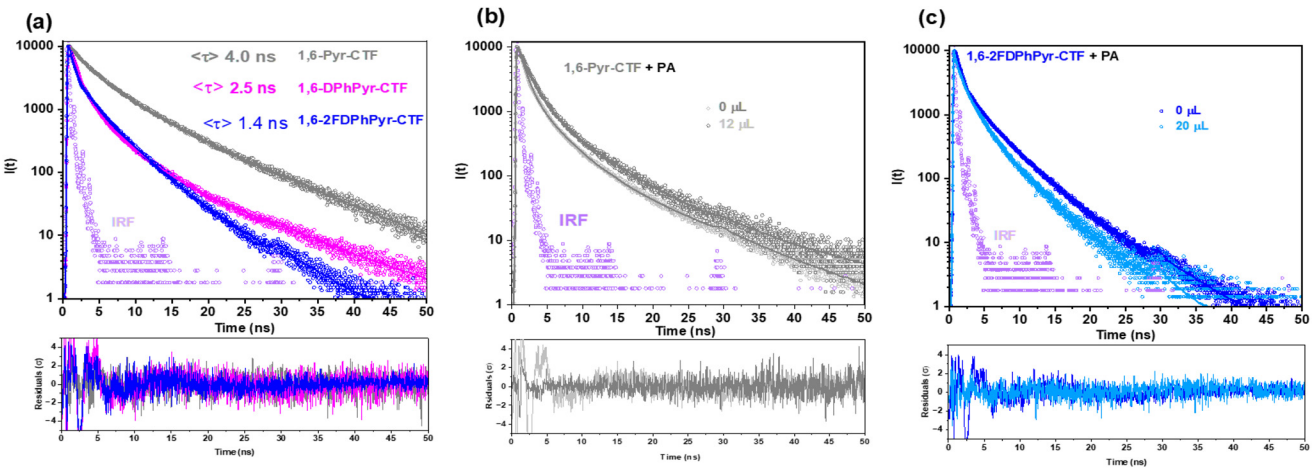

Fig. 8 Time-resolved fluorescence experiments. (a) Fluorescence lifetime decay profiles of 1,6-Pyr based CFTs; (b) and (c) in the presence of TNP solutions (0, 12 and 20 µL) (λ_{ex} = 372 nm). IRF: instrument response function. Bottom panels shows residuals from the fitting.

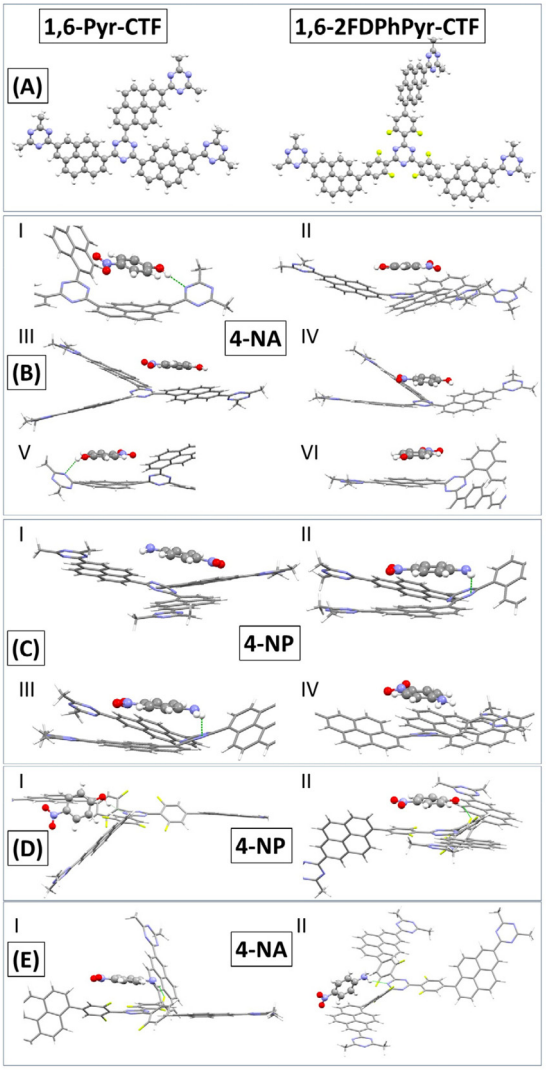

Fig. 9 (part A) Models of 1,6-Pyr-CTF of 1,6-2FDPhPyr-CTF used in the DFT calculations. Geometries of most stable adsorption configurations of 4-NA (part B) and 4-NP (part C) with the 1,6-Pyr-CTF model, and 4-NA (part D) and 4-NP (part E) with the 1,6-2FDPhPyr-CTF model. H-bonds between 4-NA and 4-NP with the triazine or fluoro atoms are highlighted in dark green color.

The conformational sampling identified two main interaction motifs between the 4-NA and 4-NP molecules with the 1,6-Pyr-CTF and 1,6-2FDPhPyr-CTF. The molecules can interact *via* π–π stacking and hydrogen-bonding. In most cases, only π–π stacking binding pattern is observed, and in fewer cases a combination of π–π stacking and hydrogen-bonding. For 4-NA interacting with the 1,6-Pyr-CTF, all configurations are similar in energy and differ by only 0.3 kJ mol^{-1}, while for 4-NP they differ up to ~10 kJ mol^{-1}. The most stable adsorption configurations are presented in Fig. 9. The computed interaction energies of both 4-NA and 4-NP with the 1,6-Pyr-CTF have similar values of ~−58.5 kJ mol^{-1}. The interactions of 4-NA and 4-NP with the 1,6-2FDPhPyr-CTF are slightly weaker compared to the 1,6-Pyr-CTF. For the most stable adsorption configurations of 4-NA with the 1,6-2FDPhPyr-CTF, the interaction energies are calculated to be ~−48 and ~−54 kJ mol^{-1}, while for 4-NP are ~−51 kJ mol^{-1}. In both molecules, the stable interaction configurations are a combination of π–π stacking and hydrogen-bonding. The DFT calculated interaction values are shown in Table S5. To further analyze the H-bonds, the Interaction Region Indicator (IRI) plots are presented in Fig. 10, where the color of the plots can qualitatively measure the strength of the H-bonds. According to the coloring scheme in the bottom part of Fig. 10, stronger interactions are depicted with isosurfaces of blue color, while green color areas represent weaker interactions. This analysis is presented for the 1,6-PYR-CTF only. H-bonds between the 4-NP with the triazine ring are always depicted in green color, while in the most stable configuration I of the 4-NA, the H-bond is depicted in blue color. This indicates qualitatively, that 4-NA interacts *via* stronger H-bonding with the 1,6-Pyr-CTF than the 4-NP. The IRI plots can also qualitatively explain the trend in the interaction energies between the configurations I and V of 4-NP (−58.8 *vs.* −43.9 kJ mol^{-1}, respectively). In Configuration I, the isosurface of the IRI plot is blue, whereas it is green for V, indicating that the H-bond is weaker in V. A general trend in the 4-NP, is that H-bonding is stronger than π–π stacking by comparing the value of I with the values of II, III, IV, and VI. However, there is no trend observed for 4-NA, where the interaction energies are computed to be almost isoenergetic.

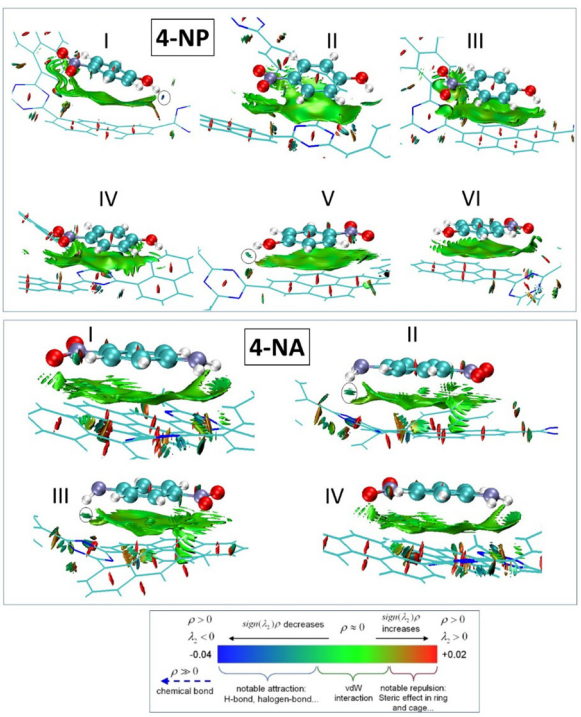

Fig. 10 IRI (Interaction Region Indicator) plots showing the interactions of 4-NP and 4-NA with the 1,6-Pyr-CTF model. Regions of H-bonding with the triazine group are shown in circles. The standard coloring method and chemical explanation of the sign(λ_2)ρ on IRI isosurfaces is also shown on the bottom part of the figure.

Conclusions

We have successfully designed and synthesized a series 1,6 pyrene-based covalent triazine frameworks (CTFs), incorporating either directly bonded pyrene-triazine units or extended pyrene-aryl-triazine linkages. Their chemical stability and strong fluorescence make them excellent candidates for fluorescence-based sensing applications. Among them, the fluorinated derivative (1,6-2FDPhPyr-CTF) exhibits the highest selectivity and sensitivity toward picric acid (TNP) and 4-nitroaniline (4-NA) with a K_{SV} value of 4.35×10^4 M^{-1} for picric acid and a detection limit of 0.15 ppm. These results highlight the positive impact of extended π-conjugation and fluorine incorporation into the aromatic ring on sensing performance. Density functional theory (DFT) analysis revealed that the enhanced sensing properties toward NACs arise from favorable π–π stacking interactions and intermolecular hydrogen bonding with nitroaromatic analytes. Overall, this work underscores the potential of nitrogen-rich 1,6 pyrene-triazines frameworks for environmental monitoring and provides valuable design principles for the rational design of efficient and selective fluorescent sensors targeting nitroaromatic pollutants.

Experimental part

Experimental details for the synthesis and characterization of 1,6 pyrene-dinitriles monomers and the corresponding pyrene-based covalent triazine frameworks can be found in the SI. Details for the computational methodology can be found in the SI. Cartesian coordinates and DFT energies of all structures are given in a separate file.

Synthesis of 1,6-Pyr-based CTFs

General procedure: to a 10 mL MW reactor equipped with a magnetic stirrer, the dinitrile monomers **1**, **2**, **3** (1 mmol, 2 eq.) and CH_2Cl_2 (1 mL) were added and cooled to 0 °C, then trifluoromethanesulfonic acid (1 mL) was slowly added. The mixture was stirred for 3 hours at 110 °C (200 W, 47 psi). After cooling to room temperature, the solution was poured into the reaction mixture is poured into a water/ice mixture (50 mL). The resulting solid was thoroughly washed with water until neutral pH was reached. The solid was filtered off and washed sequentially with water, ethanol, and THF. The product was then dried overnight at 110 °C under vacuum. Finally, it was passed through a ball mill for 5 minutes to obtain a fine powder in high yield (>70%).

Sensing studies

Stock solutions of nitro compounds were prepared at concentrations of 0.025 M in EtOH–H_2O (1 : 1) (HPLC grade). Titration experiments were performed after adding different concentrations of each analyte to 0.1 mg of a well-dispersed CTF powder in 3 mL of EtOH : H_2O (quartz cuvette, 1 cm × 1 cm). The fluorescence emission spectrum of each resultant mixture was recorded after thorough mixing by using ultrasonic treatment (5 min) to obtain a homogeneous mixture. The spectrum of each titration was repeated at least three times.

Author contributions

M Carmen Borrallo-Aniceto: investigation, methodology, formal analysis. Laura González-Aguilera, M. Luisa Ferrer: electrochemistry data. Andreas Mavrandonakis: investigation, visualization. Urbano Díaz: resources, review. Eva M. Maya: resources, review & editing. Marta Iglesias: resources, writing – review & editing, conceptualization, supervision.

Conflicts of interest

There are no conflicts to declare.

Data availability

The majority of the data is contained in the supplementary information (SI). Supplementary information is available (Synthetic procedures and characterization data of monomers and CTFs, details of sensing experiments and computational methodology). See DOI: https://doi.org/10.1039/d5lp00381d.

The rest will be made available upon request.

Acknowledgements

The authors acknowledge funding from the Spanish government through grants PID2023-146114NB-C22, PID2023-146114NB-C21, PID2021-123287OB-I00 and PID2024-155161OB-I00 (all funded by MICIU/AEI /10.13039/501100011033, and from EU FEDER), CNS2023-143965 (funded by MICIU/AEI /10.13039/501100011033 and NextGenerationEU/PRTR) and the Severo Ochoa Centres of Excellence program (Grant CEX2024-001445-S). M. P. L. acknowledges A. Guirao for TCSPC instrumental support.

References

1 X. Sun, Y. Wang and Y. Lei, Fluorescence based explosive detection: From mechanisms to sensory materials, *Chem. Soc. Rev.*, 2015, **44**, 8019–8061, DOI: 10.1039/c5cs00496a.

2 G. Feng, M. Zhu, L. Liu and C. Li, A Quantitative One-Pot Synthesis Method for Industrial Azo Pigments with Recyclable Wastewater, *Green Chem.*, 2019, **21**, 1769–1776, DOI: 10.1039/C8GC03982H.

3 A. A. Shahrivar, M. M. Rahman, D. Hagare and B. Maheshwari, Variation in Kikuyu Grass Yield in Response to Irrigation with Secondary and Advanced Treated Wastewaters, *Agric. Water Manage.*, 2019, **222**, 375–385, DOI: 10.1016/j.agwat.2019.06.012.

4 X.-S. Li, Y.-F. Li, J.-R. Wu, X.-Y. Lou, J. Han, J. Qin and Y.-W. Yang, A Color-Tunable Fluorescent Pillararene Coordination Polymer for Efficient Pollutant Detection, *J. Mater. Chem. A*, 2020, **8**, 3651–3657, DOI: 10.1039/C9TA13776A.

5 P. G. Diaz, S. Gura and J. R. Almirall, Dynamic Planar Solid Phase Microextraction-Ion Mobility Spectrometry for Rapid Field Air Sampling and Analysis of Illicit Drugs and Explosives, *Anal. Chem.*, 2010, **82**, 2826–2835, DOI: 10.1021/ac902785y.

6 N. Na, C. Zhang, M. X. Zhao, S. C. Zhang, C. D. Yang, X. Fang and X. R. Zhang, Direct detection of explosives on solid surfaces by mass spectrometry with an ambient ion source based on dielectric barrier discharge, *J. Mass Spectrom.*, 2007, **42**, 1079–1085, DOI: 10.1002/jms.1243.

7 J. W. Jaworski, D. Raorane, J. H. Huh, A. Majumdar and S. W. Lee, Evolutionary Screening of Biomimetic Coatings for Selective Detection of Explosives, *Langmuir*, 2008, **24**, 4938–4943, DOI: 10.1021/la7035289.

8 M. Gaft and L. Nagli, UV gated Raman spectroscopy for standoff detection of explosives, *Opt. Mater.*, 2008, **30**, 1739–1746, DOI: 10.1016/j.optmat.2007.11.013.

9 E. S. Forzani, D. L. Lu, M. J. Leright, A. D. Aguilar, F. Tsow, R. A. Iglesias, Q. Zhang, J. Lu, J. H. Li and N. J. Tao, A Hybrid Electrochemical-Colorimetric Sensing Platform for Detection of Explosives, *J. Am. Chem. Soc.*, 2009, **131**, 1390–1391, DOI: 10.1021/ja809104h.

10 D. Zhan, A. Saeed, Z. Li, C. Wang, Z. Yu, J. Wang, N. Zhao, W. Xu and J. Liu, Highly Fluorescent Scandium-Tetracarboxylate Frameworks: Selective Detection of Nitro-Aromatic Compounds, Sensing Mechanism, and Their Application, *Dalton Trans.*, 2020, **49**, 17737–17744, DOI: 10.1039/D0DT03781H.

11 F. Wang, C. Wei, S. Miao, Y. Tian, Y. Zhao and Z. Wang, Covalent organic frameworks: Multifunctional material in analytical chemistry, *Chem. Eng. J.*, 2024, **497**, 154915, DOI: 10.1016/j.cej.2024.154915.

12 W. Zhang, S. Liu, Q. Sun, N. Tian and Z. Wu, Synthesis of covalent organic framework materials and their application in the field of sensing, *Nano Res.*, 2024, **17**, 162–119.

13 W. He, J. Duan, H. Liu, C. Qian, M. Zhu, W. Zhang and Y. Liao, Conjugated microporous polymers for advanced chemical sensing applications, *Prog. Polym. Sci.*, 2024, **148**, 101770, DOI: 10.1016/j.progpolymsci.2023.101770.

14 Y. Yue, D. Ji, Y. Liu and D. Wei, Chemical Sensors Based on Covalent Organic Frameworks, *Chem. – Eur. J.*, 2024, **30**, e202302474, DOI: 10.1002/chem.202302474.

15 E. V. Verbitskiy, G. N. Lipunova, E. V. Nosova and V. N. Charushin, Recent advances in design of fluorescent sensors based on azole and azine derivatives towards nitroaromatic explosives and related compounds, *Dyes Pigm.*, 2025, **240**, 112848, DOI: 10.1016/j.dyepig.2025.112848.

16 P. Kuhn, M. Antonietti and A. Thomas, Porous, covalent triazine-based frameworks prepared by ionothermal synthesis, *Angew. Chem., Int. Ed.*, 2008, **47**, 3450–3453, DOI: 10.1002/anie.200705710.

17 K. Sakaushi and M. Antonietti, Carbon- and Nitrogen-Based Organic Frameworks, *Acc. Chem. Res.*, 2015, **48**, 1591–1600, DOI: 10.1021/acs.accounts.5b00010.

18 M. Liu, L. Guo, S. Jin and B. Tan, Covalent triazine frameworks: Synthesis and applications, *J. Mater. Chem. A*, 2019, **7**, 5153–5172, DOI: 10.1039/c8ta12442f.

19 C. Krishnaraj, H. S. Jena, K. Leus and P. Van Der Voort, Covalent triazine frameworks-a sustainable perspective, *Green Chem.*, 2020, **22**, 1038–1071, DOI: 10.1039/c9gc03482j.

20 S. Aggarwal and S. K. Awasthi, Emerging trends in the development and applications of triazine-based covalent organic polymers: a comprehensive review, *Dalton Trans.*, 2024, **53**, 11601–11643, DOI: 10.1039/d4dt01127a.

21 H. Wang, D. Jiang, D. Huang, G. Zeng, P. Xu, C. Lai, M. Chen, M. Cheng, C. Zhang and Z. Wang, Covalent triazine frameworks for carbon dioxide capture, *J. Mater. Chem. A*, 2019, **7**, 22848–22870, DOI: 10.1039/c9ta06847c.

22 M. C. Borrallo-Aniceto, M. Pintado-Sierra, A. Valverde-González, U. Díaz, F. Sánchez, E. M. Maya and M. Iglesias, Unveiling the potential of a covalent triazine framework based on [1]benzothieno[3,2-b][1]benzothiophene (DPhBTBT-CTF) as a metal-free heterogeneous photocatalyst, *Green Chem.*, 2023, **26**, 1975–1983, DOI: 10.1039/d3gc03529h.

23 P. Puthiaraj, Y. R. Lee, S. Zhang and W. S. Ahn, Triazine-based covalent organic polymers: Design, synthesis and applications in heterogeneous catalysis, *J. Mater. Chem. A*, 2016, **4**, 16288–16311, DOI: 10.1039/c6ta06089g.

24 Z. Qian, Z. J. Wang and K. A. I. Zhang, Covalent Triazine Frameworks as Emerging Heterogeneous Photocatalysts, *Chem. Mater.*, 2021, **33**, 1909–1926, DOI: 10.1021/acs.chemmater.0c04348.

25 D. Yadav, N. Subodh and S. K. Awasthi, Recent advances in the design, synthesis and catalytic applications of triazine-based covalent organic polymers, *Mater. Chem. Front.*, 2022, **6**, 1574–1605, DOI: 10.1039/d2qm00071g.

26 R. Sun and B. Tan, Covalent Triazine Frameworks(CTFs) for Photocatalytic Applications, *Chem. Res. Chin. Univ.*, 2022, **38**(2), 310–324, DOI: 10.1007/s40242-022-1468-4.

27 P. Xiong, S. Zhang, R. Wang, L. Zhang, Q. Ma, X. Ren, Y. Gao, Z. Wang, Z. Guo and C. Zhang, Covalent triazine frameworks for advanced energy storage: challenges and new opportunities, *Energy Environ. Sci.*, 2023, **16**, 3181–3213, DOI: 10.1039/d3ee01360j.

28 F. Xu, S. Yang, G. Jiang, Q. Ye, B. Wei and H. Wang, Fluorinated, Sulfur-Rich, Covalent Triazine Frameworks for Enhanced Confinement of Polysulfides in Lithium-Sulfur Batteries, *ACS Appl. Mater. Interfaces*, 2017, **9**, 37731–37738, DOI: 10.1021/acsami.7b10991.

29 E. Saputra, B. A. Prawiranegara, H. Sugesti, M. W. Nugraha and P. S. Utama, Covalent triazine framework: Water treatment application, *J. Water Process Eng.*, 2022, **48**, 102874, DOI: 10.1016/j.jwpe.2022.102874.

30 S. Pourebrahimi and M. Pirooz, Functionalized covalent triazine frameworks as promising platforms for environ-

mental remediation: A review, *Clean. Eng. Technol.*, 2022, **2**, 100012, DOI: 10.1016/j.clce.2022.100012.

31 P. M. C. Matias, D. Murtinho and A. J. M. Valente, Triazine-Based Porous Organic Polymers: Synthesis and Application in Dye Adsorption and Catalysis, *Polymers*, 2023, **15**, 1815, DOI: 10.3390/polym15081815.

32 S. Pourebrahimi and M. Pirooz, Synthesis of a novel free-standing conjugated triazine-based microporous membrane through superacid-catalyzed polymerization for superior CO_2 separation, *Chem. Eng. J. Adv.*, 2022, **11**, 100315, DOI: 10.1016/j.ceja.2022.100315.

33 B. Liang, X. He, J. Hou, L. Li and Z. Tang, Membrane Separation in Organic Liquid: Technologies, Achievements, and Opportunities, *Adv. Mater.*, 2019, **31**, 1–14, DOI: 10.1002/adma.201806090.

34 H. Hong, N. Wu, M. Han, Z. Guo, H. Zhan, S. Du and B. Chen, An anthracene based conjugated triazine framework as a luminescent probe for selective sensing of p-nitroaniline and Fe(III) ions, *Mater. Chem. Front.*, 2021, **5**, 6568–6574, DOI: 10.1039/d1qm00686j.

35 G. Sathiyan, G. Venkatesan, S. K. Ramasamy, J. Lee and S. Barathi, Recent progress in triazine-based fluorescent probes for detecting hazardous nitroaromatic compounds, *J. Environ. Chem. Eng.*, 2024, **12**, 112804, DOI: 10.1016/j.jece.2024.112804.

36 H. Bhambri, S. Khullar, Sakshi and S. K. Mandal, Nitrogen-rich covalent organic frameworks: A promising class of sensory materials, *Mater. Adv.*, 2022, **3**, 19–124, DOI: 10.1039/d1ma00506e.

37 T. M. Figueira-Duarte and K. Müllen, Pyrene-based materials for organic electronics, *Chem. Rev.*, 2011, **111**, 7260–7314, DOI: 10.1021/cr100428a.

38 X. Feng, J. Y. Hu, C. Redshaw and T. Yamato, Functionalization of Pyrene to Prepare Luminescent Materials—Typical Examples of Synthetic Methodology, *Chem. – Eur. J.*, 2016, **22**, 11898–11916, DOI: 10.1002/chem.201600465.

39 H. M. Kim, Y. O. Lee, C. S. Lim, J. S. Kim and B. R. Cho, Two-Photon Absorption Properties of Alkynyl-Conjugated Pyrene Derivatives, *J. Org. Chem.*, 2008, 5127–5130, DOI: 10.1021/jo800363v.

40 R. S. Sprick, J. X. Jiang, B. Bonillo, S. Ren, T. Ratvijitvech, P. Guiglion, M. A. Zwijnenburg, D. J. Adams and A. I. Cooper, Tunable organic photocatalysts for visible-light-driven hydrogen evolution, *J. Am. Chem. Soc.*, 2015, **137**, 3265–3270, DOI: 10.1021/ja511552k.

41 M. Jung, J. Lee, H. Jung, S. Kang, A. Wakamiya and J. Park, Highly efficient pyrene blue emitters for OLEDs based on substitution position effect, *Dyes Pigm.*, 2018, **158**, 42–49, DOI: 10.1016/j.dyepig.2018.05.024.

42 C. C. Yu, K. J. Jiang, J. H. Huang, F. Zhang, X. Bao, F. W. Wang, L. M. Yang and Y. Song, Novel pyrene-based donor-acceptor organic dyes for solar cell application, *Org. Electron.*, 2013, **14**, 445–450, DOI: 10.1016/j.orgel.2012.12.013.

43 S. Zhang, Y. Moustafa and Q. Huo, Different interaction modes of biomolecules with citrate-capped gold nanoparticles, *ACS Appl. Mater. Interfaces*, 2014, **6**, 21184–21192, DOI: 10.1021/am506112u.

44 Y. Shi, Z. Li, Y. Fang, J. Sun, M. Zhao and Y. Song, Ultrafast third-order nonlinear optical response of pyrene derivatives, *Opt. Laser Technol.*, 2017, **90**, 18–21, DOI: 10.1016/j.optlastec.2016.11.003.

45 Q. Fang, J. Li, S. Li, R. Duan, S. Wang, Y. Yi, X. Guo, Y. Qian, W. Huang and G. Yang, Thermally populated "bright" states for wide-range and high temperature sensing in air, *Chem. Commun.*, 2017, **53**, 5702–5705, DOI: 10.1039/c7cc00551b.

46 B. B. Ma, G. F. Feng, P. C. Zhao, F. F. Chang and W. Huang, Asymmetric imidazole/pyrene/pyrazine based D-π-A compounds showing visualized acidichromism and near-infrared electrochromism, *Tetrahedron Lett.*, 2015, **56**, 6912–6914, DOI: 10.1016/j.tetlet.2015.10.100.

47 J. Chao, H. Wang, Y. Zhang, C. Yin, F. Huo, K. Song, Z. Li, T. Zhang and Y. Zhao, A novel '"donor-π-acceptor"' type fluorescence probe for sensing pH: mechanism and application in vivo, *Talanta*, 2017, **174**, 468–476, DOI: 10.1016/j.talanta.2017.06.051.

48 Z. M. Sahin, D. Alimli, M. M. Tonta, M. E. Kose and F. Yilmaz, Highly sensitive and reusable mercury(II) sensor based on fluorescence quenching of pyrene moiety in polyacrylamide-based cryogel, *Sens. Actuators, B*, 2017, **242**, 362–368, DOI: 10.1016/j.snb.2016.11.048.

49 C. Wu, Y. Ikejiri, J. L. Zhao, X. K. Jiang, X. L. Ni, X. Zeng, C. Redshaw and T. Yamato, A pyrene-functionalized triazole-linked hexahomotrioxacalix[3]arene as a fluorescent chemosensor for Zn^{2+} ions, *Sens. Actuators, B*, 2016, **228**, 480–485, DOI: 10.1016/j.snb.2016.01.051.

50 H. L. Barros, M. A. Esteves and M. J. Brites, Synthesis, photophysical and electrochemical properties of π-conjugated pyrene based down-shifting molecules with fluorinated aryl groups, *Dyes Pigm.*, 2023, **213**, 111103, DOI: 10.1016/j.dyepig.2023.111103.

51 K. Inoue, R. Kawakami, M. Murakami, T. Nakayama, S. Yamamoto, K. Inoue, T. Tsuda, K. Sayama, T. Imamura, D. Kaneno, S. Hadano, S. Watanabe and Y. Niko, Synthesis and photophysical properties of a new push-pull pyrene dye with green-to-far-red emission and its application to human cellular and skin tissue imaging, *J. Mater. Chem. B*, 2022, **10**, 1641–1649, DOI: 10.1039/d1tb02728j.

52 J. Merz, M. Dietz, Y. Vonhausen, F. Wöber, A. Friedrich, D. Sieh, I. Krummenacher, H. Braunschweig, M. Moos, M. Holzapfel, C. Lambert and T. B. Marder, Synthesis, Photophysical and Electronic Properties of New Red-to-NIR Emitting Donor–Acceptor Pyrene Derivatives, *Chem. – Eur. J.*, 2020, **26**, 438–453, DOI: 10.1002/chem.201904219.

53 A. Kathiravan, M. Panneerselvam, K. Sundaravel, N. Pavithra, V. Srinivasan, S. Anandan and M. Jaccob, Unravelling the effect of anchoring groups on the ground and excited state properties of pyrene using computational

and spectroscopic methods, *Phys. Chem. Chem. Phys.*, 2016, **18**, 13332–13345, DOI: 10.1039/c6cp00571c.

54 M. W. Lee, J. Y. Kim, H. J. Son, J. Y. Kim, B. Kim, H. Kim, D. K. Lee, K. Kim, D. H. Lee and M. J. Ko, Tailoring of Energy Levels in D-π-A Organic Dyes via Fluorination of Acceptor Units for Efficient Dye-Sensitized Solar Cells, *Sci. Rep.*, 2015, **5**, 7711, DOI: 10.1038/srep07711.

55 X. Gong, D. Heeran, Q. Zhao, C. Zheng, D. S. Yufit, G. Sandford and D. Gao, Synthesis of Fluoro and Cyanoaryl-Containing Pyrene Derivatives and their Optical and Electrochemical Properties, *Asian J. Org. Chem.*, 2019, **8**, 722–730, DOI: 10.1002/ajoc.201900018.

56 M. C. Borrallo-aniceto, B. Fuerte-díez, A. Valverde-González, M. L. Ferrer, M. P. Lillo, U. Díaz, E. M. Maya, L. Gonzalez and M. Iglesias, Effect of functionalization on axially substituted 2,7-pyrene covalent triazine frameworks for dual sensing applications, *Mater. Today Chem.*, 2025, **50**, 103149, DOI: 10.1016/j.mtchem.2025.103149.

57 F.-W. Yen and Ch.-H. Ch. Miaoli, Light emitting material for organic electroluminescence device US 10,636,977 B2, Apr 28 2020. Samsung Display-Kr2015/29430, 2015, A, Luminescence Technology- Cn107652307, 2018, A, Valiant - CN105131938, 2017, B.

58 F. Li, M. Pan, Q. He, Q. Zhou, Q. Tang and C. Gong, Ester-functionalized pyrene derivatives: Effects of ester substituents on photophysical, electrochemical, electrochromic, and electrofluorochromic properties, *Dyes Pigm.*, 2022, **201**, 110203, DOI: 10.1016/j.dyepig.2022.110203.

59 T. M. Geng, C. Zhang, C. Hu, M. Liu, Y. T. Fei and H. Y. Xia, Synthesis of 1,6-disubstituted pyrene-based conjugated microporous polymers for reversible adsorption and fluorescence sensing of iodine, *New J. Chem.*, 2020, **44**, 2312–2320, DOI: 10.1039/c9nj05509f.

60 X. Gong, X. Xie, N. Chen, C. Zheng, J. Zhu, R. Chen, W. Huang and D. Gao, Two Symmetrically Bis-substituted Pyrene Derivatives: Synthesis, Photoluminescence, and Electroluminescence, *Chin. J. Chem.*, 2015, **33**, 967–973, DOI: 10.1002/cjoc.201500385.

61 A. Bhunia, D. Esquivel, S. Dey, R. Fernández-Terán, Y. Goto, S. Inagaki, P. Van Der Voort and C. Janiak, A photoluminescent covalent triazine framework: CO2 adsorption, light-driven hydrogen evolution and sensing of nitroaromatics, *J. Mater. Chem. A*, 2016, **4**, 13450–13457, DOI: 10.1039/c6ta04623a.

62 X. Ma, F. Tao, Y. Zhang, T. Li, F. M. Raymo and Y. Cui, Detection of nitroaromatic explosives by a 3D hyperbranched σ-π Conjugated polymer based on a POSS scaffold, *J. Mater. Chem. A*, 2017, **5**, 14343–14354, DOI: 10.1039/c7ta04351a.

63 N. Jiang, G. Li, W. Che, D. Zhu, Z. Su and M. R. Bryce, Polyurethane derivatives for highly sensitive and selective fluorescence detection of 2,4,6-trinitrophenol (TNP), *J. Mater. Chem. C*, 2018, **6**, 11287–11291, DOI: 10.1039/c8tc04250k.

64 A. S. Tanwar, S. Hussain, A. H. Malik, M. A. Afroz and P. K. Iyer, Inner Filter Effect Based Selective Detection of Nitroexplosive-Picric Acid in Aqueous Solution and Solid Support Using Conjugated Polymer, *ACS Sens.*, 2016, **1**, 1070–1077, DOI: 10.1021/acssensors.6b00441.

65 K. S. Asha, K. Bhattacharyya and S. Mandal, Discriminative detection of nitro aromatic explosives by a luminescent metal-organic framework, *J. Mater. Chem. C*, 2014, **2**, 10073–10081, DOI: 10.1039/c4tc01982b.

66 S. Chen, Y. L. Yu and J. H. Wang, Inner filter effect-based fluorescent sensing systems: A review, *Anal. Chim. Acta*, 2018, **999**, 13–26, DOI: 10.1016/j.aca.2017.10.026.

67 B. W. Wang, K. Jiang, J. X. Li, S. H. Luo, Z. Y. Wang and H. F. Jiang, 1,1-Diphenylvinylsulfide as a Functional AIEgen Derived from the Aggregation-Caused-Quenching Molecule 1,1-Diphenylethene through Simple Thioetherification, *Angew. Chem., Int. Ed.*, 2020, **59**, 2338–2343, DOI: 10.1002/anie.201914333.